Protocols for studying the time-dependent mechanical response of viscoelastic materials using spherical indentation stress-strain curves

M. T. Abba & S. R. Kalidindi

Mechanics of Time-Dependent Materials

An International Journal Devoted to the Time-Dependent Behaviour of Materials and Structures

ISSN 1385-2000

Mech Time-Depend Mater DOI 10.1007/s11043-020-09472-y





Your article is protected by copyright and all rights are held exclusively by Springer Nature B.V.. This e-offprint is for personal use only and shall not be self-archived in electronic repositories. If you wish to self-archive your article, please use the accepted manuscript version for posting on your own website. You may further deposit the accepted manuscript version in any repository, provided it is only made publicly available 12 months after official publication or later and provided acknowledgement is given to the original source of publication and a link is inserted to the published article on Springer's website. The link must be accompanied by the following text: "The final publication is available at link.springer.com".



Mech Time-Depend Mater https://doi.org/10.1007/s11043-020-09472-v



Protocols for studying the time-dependent mechanical response of viscoelastic materials using spherical indentation stress-strain curves

M.T. Abba¹ · S.R. Kalidindi¹

Received: 2 June 2019 / Accepted: 1 October 2020

© Springer Nature B.V. 2020

Abstract Spherical nanoindentation has been used successfully to extract meaningful indentation stress-strain curves in hard materials such as metals and ceramics. These methods have not yet been applied on viscoelastic-viscoplastic polymer samples. This study explores the potential of the current spherical nanoindentation analysis protocols in extracting indentation stress-strain curves and viscoelastic properties on samples exhibiting time-dependent material response at room temperature. These new protocols were tested on polymethyl methacrylate, polycarbonate, and low-density polyethylene. The properties extracted under different loading rates and indenter tip sizes conditions were observed to be consistent. It is further demonstrated that it is possible to recover the compression stress-strain curves for polymethyl methacrylate and low-density polyethylene from the measured indentation stress-strain curves. This study establishes some of the foundations needed for the development of protocols needed to reliably investigate the local time-dependent mechanical response of materials using spherical nanoindentation.

Keywords Nanoindentation \cdot Viscoelasticity \cdot Stress-strain \cdot Microscale \cdot Finite element analysis

1 Introduction

Optimizing the overall mechanical properties of most advanced materials requires a good understanding of the mechanical properties of its microscale constituents. This task requires the development and validation of novel multi-resolution mechanical characterization assays (Hemker and Sharpe 2007; Jaya and Alam 2013; Srikar and Spearing 2003). In addition to being able to measure the mechanical properties in very small volumes typical of the sizes of the microscale constituents in advanced materials, it is desirable to develop methods capable of high-throughput testing. This is essential to obtain critical information on the very

S.R. Kalidindi surya.kalidindi@me.gatech.edu

Published online: 23 October 2020

George W. Woodruff School of Mechanical Engineering, Georgia Institute of Technology, Atlanta, GA 30332-0405, USA



large variety of potential microscale constituents that could be found in advanced material systems (Kalidindi et al. 2017). Nanoindentation offers tremendous promise in addressing this critical need, and has been successfully employed to study the microscale properties of metal and ceramic constituents in advanced material systems (Khosravani et al. 2020; Weaver and Kalidindi 2016; Fischer-Cripps 2002). There is a critical need to extend these protocols to measuring the time-dependent mechanical responses of the viscoelastic constituents in complex material systems.

More specifically, modern nanoindenters possess high load resolution and depth sensing capabilities, and can be used to characterize the local mechanical behavior in materials at very small spatial resolutions ranging from ~ 100 nm to ~ 500 µm. Moreover, recently developed instrumented spherical indentation data analysis methods have demonstrated a tremendous potential to transform the raw load-displacement data into very meaningful indentation stress-strain curves (Kalidindi and Pathak 2008; Pathak and Kalidindi 2015; Weaver and Kalidindi 2016; Vachhani et al. 2016; Patel and Kalidindi 2017). These protocols have been able to capture the local loading and unloading elastic moduli, the local indentation yield strengths, and some characteristics of the post-yield behavior in several samples (Pathak et al. 2008; Pathak et al. 2009a). The validity of these protocols has been critically evaluated using finite element models (Donohue et al. 2012; Patel and Kalidindi 2016). By recovering indentation stress-strain curves from the measured indentation load-displacement data, we can get a much more reliable and objective comparison of material behavior between different samples or between different locations in the sample, compared to the conventional hardness measurements. These new protocols have thus far been explored mostly on materials that do not experience significant timedependent deformation.

A salient feature of the methods described above is that they isolate the initial elastic loading segment (in the initial contact of the indenter with the sample), and analyze it rigorously using Hertz's theory (Kalidindi and Pathak 2008). It is extremely critical to establish the elastic stiffness of the virgin sample, as any amount of plastic deformation changes the unloaded sample surface geometry and adds significant error to the proper analyses of the indentation data using Hertz's theory (Pathak and Kalidindi 2015). In the indentation analyses protocols, continuous and accurate measurement of the elastic stiffness (as will be discussed later) is central to the extraction of the indentation stress-strain curves, even into the inelastic regime well beyond the elastic regime. This is because only the elastic stiffness gives an estimate of the indenter-sample contact geometry that is fully consistent with Hertz's theory (Donohue et al. 2012). Any other direct or indirect estimate of the contact geometry results in an erroneous application of Hertz's theory for indentation analyses. Indeed, this requirement has posed major challenges to the conventional protocols for the extraction of indentation stress-strain curves from the raw load-displacement measurements, and has only been circumvented with the high resolution measurement capabilities of modern nanoindenters. In this regard, it should be noted that the initial elastic segment has been successfully isolated and analyzed with only spherical indenters, as the sharp indenters usually produce inelastic deformation as soon as they touch the sample surface. For the present study, our goal is to extend the previously established spherical nanoindentation stress-strain protocols to materials that exhibit viscoelasticity at room temperature. This work lays a foundation for future work aimed at studies of viscoelastic and viscoplastic properties of individual mesoscale constituents of composite material systems, including interphases.

The protocols developed in this work are demonstrated on three commercially available polymers (polymethyl methacrylate (PMMA), polycarbonate (PC), and low-density polyethylene (LDPE)) using three different indenter tip radii (16 μm, 100 μm, and 1500 μm).



The properties and stress-strain curves obtained from nanoindentation are compared against results obtained from conventional simple (uniaxial) compression tests performed on the same polymers at a similar strain rate. Finite element (FE) simulations of spherical nanoindentation and uniaxial compression are also performed to understand the differences in the indentation and simple compression responses in these materials.

2 Background: viscoelastic indentations and analyses

Most prior studies on nanoindentation of polymers have focused on extracting the creep compliance or relaxation modulus, where these quantities are expressed either using a mechanical model or a Prony series representation (Huang and Lu 2006; Cheng et al. 2005; Huang and Lu 2007). These studies have generally used sharp indenter tips (e.g., Berkovich or conical) (Briscoe et al. 1998; Jakes et al. 2012; Cheng and Cheng 2005b). In some studies, spherical tips were used to investigate the viscoelastic behavior of different polymers (Zhou and Lu 2010; Knauss et al. 2008; Martynova 2016). Because of viscoelasticity, the loading conditions imposed in the indentation play an important role. The most common approach has been to ramp the load or displacement to a preset value, and holding it for some time. The relaxation modulus or creep compliance is then extracted from the hold regime using established viscoelastic indentation models. It is important to recognize that a step loading condition is impossible to implement practically, and therefore it is important to account for the ramp load before the hold in the analyses of the raw data. Oyen (2005) has demonstrated a "ramp correction factor" for the exponential decay terms to address this challenge. As mentioned earlier, there may be substantial amount of plastic deformation imposed on the sample in the initial ramp, especially with the use of sharp indenters. As already noted, any amount of plastic deformation adds significant errors to the analyses based on Hertz's theory because of the changes induced in the unloaded sample surface geometry (its radius is no longer known a priori). Because of such errors, the properties extracted from the hold regime in these experiments may not represent faithfully the properties of the as-received sample. A number of indentation studies have also explored the response of a viscoelastic material to dynamic (oscillatory) loading at different frequencies (Huang et al. 2004; Odegard et al. 2005; Jäger and Lackner 2008) in order to estimate the storage and loss moduli.

Theories of linear viscoelastic indentation started in the mid-1950s with the work of Lee (1956), Radok (Lee and Radok 1960), Hunter (1960), Graham (1965), and Ting (1966). They developed an approach for finding the viscoelastic solution in cases where the corresponding solution for the purely elastic case is already known (referred as the viscoelastic correspondence principle). Using these theories, the load-displacement relationship for the frictionless indentation of an isotropic, linear viscoelastic, solid using a rigid indenter exhibiting a quadratic axisymmetric surface geometry in the contact region can be expressed in two equivalent forms as

$$h^{3/2}(t) = \frac{3(1-v^2)}{4\sqrt{R_{eff}}} \int_0^t J(t-\tau) \frac{dP(\tau)}{d\tau} d\tau$$
 (1)

$$P(t) = \frac{4\sqrt{R_{eff}}}{3(1-v^2)} \int_0^t E(t-\tau) \frac{dh^{\frac{3}{2}}(\tau)}{d\tau} d\tau$$
 (2)



where P(t) and h(t) denote the load and displacement, respectively, as functions of time. In Eq. (1) and Eq. (2), J(t), E(t) and v denote the isotropic creep compliance, isotropic relaxation modulus and the time-independent Poisson's ratio, respectively, of the material being indented. R_{eff} denotes an effective curvature of the indenter-sample contact defined through $1/R_{eff} = 1/R_i + 1/R_s$, where R_i and R_s denote the radii of curvature of the indenter and the sample, respectively, in the undeformed condition. For the initial elastic indentation of a flat sample, $R_{eff} = R_i$. However, if one loads the sample beyond its elastic limit, R_{eff} continuously changes with the imposed deformation. The central challenge in analyzing indentation datasets stem from the difficulty of measuring or estimating the change in R_{eff} beyond the very small initial elastic loading segment (Pathak and Kalidindi 2015). An important result from the linear viscoelastic indentation theory is the relationship between the indentation depth and the contact area (a) expressed as (Cheng and Cheng 2005a)

$$a(t) = \sqrt{h(t)R_{eff}} \tag{3}$$

Note that this relationship is the same as the original Hertz model for the case of the elastic indentation.

Most modern indenters also provide a continuous stiffness measurement (CSM). This signal provides a reliable estimate of the elastic stiffness (S) by imposing a small, sinusoidally varying load on top of the DC signal that drives the indenter, allowing for a continuous measurement of the resulting amplitude and phase of the displacement oscillation (Li and Bhushan 2002). In elastic indentation, this measurement of the stiffness allows for a reliable estimate of the contact radius using the relationship (Donohue et al. 2012; Kalidindi and Pathak 2008)

$$a = \frac{S}{2E_{eff}} \tag{4}$$

$$\frac{1}{E_{eff}} = \frac{1 - v_s^2}{E_s} + \frac{1 - v_i^2}{E_i} \tag{5}$$

where E_{eff} is called the effective elastic modulus and ν is the Poisson's ratio, while subscripts s and i refer to the specimen and indenter, respectively. It is not yet clear if this equation needs to be modified in any way for the viscoelastic indentation. We will explore this question critically in this study through suitably designed FEM simulations.

Creep compliance used in Eq. (1) is usually expressed as a time series called the Prony series (Lakes 2009):

$$J(t) = J_{\infty} - \sum_{i=1}^{N} J_i e^{-t/\tau_{ci}}$$
 (6)

where J_{∞} is the steady state creep compliance of the system and J_i and τ_{ci} are the compliances and time constants associated with the underlying viscoelastic mechanisms of deformation in the material. Note that the instantaneous creep compliance, J_0 , can be computed from Eq. (6) by setting t = 0. In an analogous manner, one can express the relaxation modulus as

$$E(t) = E_{\infty} + \sum_{i=1}^{N} E_i e^{-t/\tau_{ri}}$$
 (7)

where E_{∞} is the steady state stiffness of the system and E_i are the stiffnesses capturing the viscoelastic behavior of the material. The creep compliance and the relaxation modulus are



related to each other through

$$\int_0^t J(t-\tau)E(\tau)d\tau = \int_0^t E(t-\tau)J(\tau)d\tau = t \tag{8}$$

It is noted that the Prony series is a common method of describing viscoelastic behavior that is available in most commercial finite element software. In the present work, we implemented this description of the viscoelastic material in a finite element model of spherical indentation using the commercial software ABAQUS (Dassault Systemes Simulia Corp. 2014). In this implementation, Prony series was defined for both the shear and the bulk relaxation moduli by assuming that the Poisson's ratio is a constant and that $G(t) = E(t)/2(1 + \nu)$ and $K(t) = E(t)/3(1 - 2\nu)$ (Brinson and Brinson 2008; Gauthier 1995; Lakes and Wineman 2006).

3 Material and methods

3.1 Materials

All the polymers used in this study were obtained from McMaster-Carr (Elmhurst, IL). For nanoindentation, the specimen were obtained from a 1.25 inch diameter extruded rods of PMMA (density 0.043 lbs/in³; glass transition temperature 105 °C), PC (density 0.045 lbs/in³; glass transition temperature 145 °C), and LDPE (density 0.033 lbs/in³; glass transition temperature -125 °C). For compression tests, the PMMA and PC specimen were taken from extruded rods of approximately 0.625 in diameter and 1.1 in length and the LDPE specimen from extruded rods of approximately 1 in diameter and 2 in length. PMMA specimens were annealed at 110 °C and PC specimens were annealed at 150 °C. All the specimens were annealed in a Thermo Scientific Lindberg/Blue MTM MoldathermTM box furnace (Waltham, MA) for two hours and then slowly cooled down to room temperature at a rate of 5 °C/hr. The nanoindentation specimen were cut perpendicular to the extruded direction using an Allied TechCut 5TM (Rancho Dominguez, CA) precision sectioning machine and then polished using silicon carbide papers of decreasing grit sizes (320, 800, 1200, 2400, and 4000 grit) using a StruersTegramin-30 (Cleveland, OH). Each polishing step except the 4000 grit was performed for 2 minutes, followed by washing to remove debris. The 4000 grit polishing was performed for 6 minutes. This was followed by polishing with a 1 µm alcohol based diamond suspension (Struers DP-Suspension) for 20 minutes and a 0.05 µm colloidal silica suspension (Buehler MasterMet) for 20 minutes.

3.2 Uniaxial compression tests

Compression tests were performed on an MTI Phoenix Universal Testing Machine with a 20,000 lb load cell. Tests were performed according to ASTM standard D695 for testing plastics (D695-10 2010) at a speed of 0.05 in/min. Displacement was measured using a capacitance gage and all load-displacement data was converted to true stress-strain curves. At least five samples were tested for each material with the data reported as mean \pm standard deviation.



3.3 Indentation tests

The indentation tests were performed on an Agilent G200 (Keysight Technologies Inc., Santa Rosa, CA) Nano Indenter with an XP head. The indenter has a maximum load of 500 mN with a high load option of 10 N and a load resolution of 50 nN. The maximum indentation depth achievable is greater than 500 µm with a resolution of less than 0.01 nm. The indents are performed on the polished surfaces of the polymers and the spherical diamond tips used have radii of 16 µm, 100 µm, and 1500 µm. Prior to use, the tips were tested on Silica standards to confirm that the measured mechanical properties are close to the expected values. The tips were also visually inspected in the SEM for defects or dirt. Since changes in temperature can cause expansion or shrinkage of materials leading to errors in measurement, the indenter measures a thermal drift before each test by holding the indenter on the surface of the material and measuring any changes in displacement. All tests were performed after the measured indenter drift rate reached and maintained a value less than 0.05 nm/s. The machine applies a drift correction as part of the standard operating procedure. CSM corrections were applied to the displacement, load, and stiffness of all the tests using protocols described in previously published papers (Vachhani et al. 2013; Pharr et al. 2009). The stress-strain curves extracted in this study are from indentations performed at rates of 0.05 s^{-1} and 0.5 s^{-1} , defined as the loading rate, dP/dt, divided by the measured load, P. At least five curves were used to extract any mechanical properties in this study.

3.4 Finite element model of spherical indentation

In prior studies (Donohue et al. 2012; Patel and Kalidindi 2016; Bouzakis et al. 2002), finite element models were found invaluable in improving the understanding and analyses of the measurements obtained from indentation experiments. This is mainly because they allow us to evaluate critically the consequences of many assumptions and idealizations made in the analyses of the measured datasets, such as the definitions of indentation stress and indentation strain, the estimation of the contact radius, and the relationships between indentations stress-strain curves and simple compression stress-strain curves.

A two-dimensional axisymmetric finite element model of the spherical indentation shown in Fig. 1 was produced using the commercial finite element code ABAQUS (Dassault Systemes Simulia Corp. 2014). The indenter is assumed to be rigid with a radius of 10 µm, and the sample is assumed to exhibit an isotropic constitutive response. The sample was meshed using four-noded axisymmetric (CAX4) elements. The sample is constrained from moving in the 1-direction (x-axis) along the axis of symmetry and in the 2-direction (y-axis) along the bottom surface (see Fig. 1). The highest mesh density was achieved in the region where highest stresses or strains were expected. A mesh density higher than 64 elements/µm (along the 1-direction) is used for all simulations in this zone. A downward vertical displacement condition was imposed on the node at the center of the indenter, which was tied to the surface of the indenter. Contact between the sample and indenter was defined as a hard surface-tosurface contact with the indenter as the master surface and the sample as the slave surface. The FE model was validated by comparing the predicted results in elastic and viscoelastic indentations against the known theoretical solutions (see also Eq. (2)). The FE result showed good agreement with the analytical solutions, thereby validating the FE model developed in this study for simulating indentation.



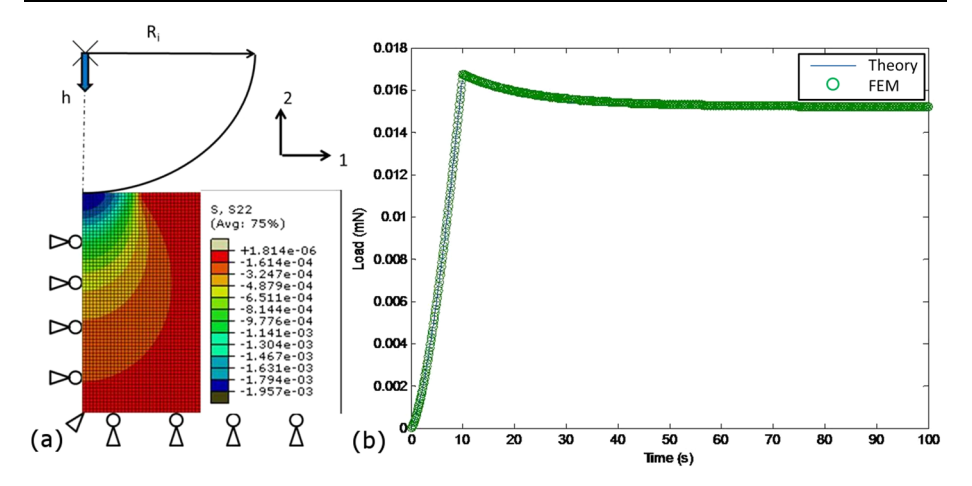


Fig. 1 a) Schematic of indenter, sample, and boundary conditions used for finite element simulations. b) An example of a ramp and hold nanoindentation simulation compared to the theoretical solution obtained from Eq. (2)

3.5 Nanoindentation protocols for viscoelastic materials

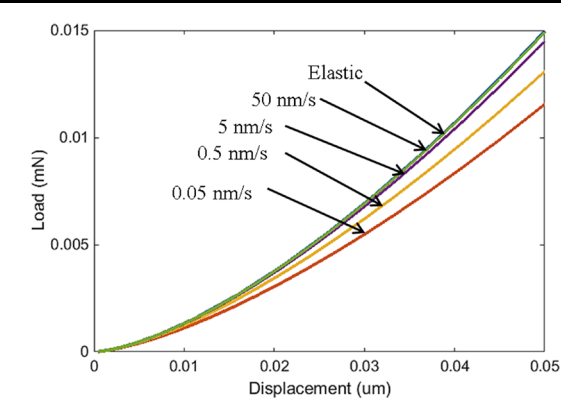
New indentation protocols have been developed in this work for studying viscoelastic response of materials. These will be presented next, and comprise five distinct steps. The first step is designed to determine if the material has a sufficiently dominant viscous component to affect its deformation behavior. This is particularly useful for new materials for which prior information is not adequate. In some materials, the time constants of the viscous response are very small, allowing us to treat the material simply as an elasticplastic material. The first step allows us to make a decision in this regard. The second step is designed to determine which region of the indentation load-displacement curve is viscoelastic. Any properties extracted assuming viscoelastic behavior should come from this region. The third step aims to extract the creep compliance after an indentation has been performed. The fourth step ensures that the initial portion of the load-displacement curve is corrected for the zero-point. A zero-point identifies the point of effective initial contact between the indenter and the sample. In prior work (Kalidindi and Pathak 2008; Donohue et al. 2012), it has been clarified that the point of effective contact is the point on the measured load-displacement curve that produces the best fit of the initial elastic (extended here to viscoelastic) portion to the theoretically expected response. This concept is useful to circumvent unavoidable consequences from sample preparation artifacts such as surface roughness or very small disturbed surface layers. The identification of the zero-point has a major influence on the extracted indentation stress-strain curves. The final step is to calculate the stress-strain curves from the nanoindentation data collected. All of the steps are described in detail next.

3.5.1 Step 1: determine material viscoelasticity

Material viscoelasticity can be studied simply by indenting the sample at different displacement/loading rates and examining the differences in the measured load-displacement curves in the viscoelastic regime. The expected trends can also be studied using the FE model. This



Fig. 2 FE simulation of indentation loading on LDPE at different displacement rates



is illustrated in Fig. 2 using the viscoelastic material properties obtained from tests on LDPE (presented in the next section), expressed as a two-term Prony series

$$E(t) = 0.15 + 0.057e^{-0.091t} + 0.043e^{-0.0094t} \text{ GPa}$$
(9)

The material properties used for the fully elastic simulations were the steady state stiffness, 0.25 GPa, and LDPE's Poisson's ratio, 0.45. In these simulations, the maximum indentation depth was selected as 50 nm, and the indentation rates were selected as 50 nm/s, 5 nm/s, 0.5 nm/s, and 0.05 nm/s. As seen from Fig. 2, the material responds differently at the different indentation rates. At the high displacement rates, the response is almost identical to the elastic case. This is because the time it takes to reach the specified displacement is lower than the material's time constants, thus not giving the material enough time to relax. At a lower displacement rate, the material has enough time to relax thus the response is lower.

3.5.2 Step 2: determine viscoelastic region

This can be determined by loading and unloading the material at increasing loads using the same loading rate. At the end of each unload a small load is held on the material and the displacement is allowed to recover. The goal is to observe where the displacement stops decreasing and how this residual displacement changes at different loads. Ideally, if the indentation is still within the viscoelastic regime, the residual displacement will be close to zero at the different maximum loads. For highly viscoelastic materials, it may take much longer for the material to return to its initial condition. Thus it is very difficult in practice to quantify the exact point of yield on the load-displacement curve. Our goal here is to make an educated guess. Since this is not an exact value, it is generally better to be conservative in identifying the load or displacement levels where the viscoelastic behavior of the material ends. It is important to avoid plasticity because it results in dramatic changes to $R_{\rm eff}$ (see Eq. (1)). As soon as plasticity initiates, one needs a different set of protocols to estimate the contact radius and its evolution through the entire indentation test (Pathak and Kalidindi 2015; Pathak et al. 2008; Pathak et al. 2009b).

Each sample studied in this work was loaded and unloaded at the same rate with three or four different maximum loads. Before completely unloading the material, a small preset load was left on the material for an extended period of time. Using the $100 \mu m$ radius indenter tip PMMA and PC were loaded at a loading rate of $2.5 \mu m$ /s with maximum loads of $40 \mu m$, $80 \mu m$, $160 \mu m$, and $320 \mu m$ for PMMA and $20 \mu m$, $40 \mu m$, $80 \mu m$, and $320 \mu m$ for PMMA and $20 \mu m$, $40 \mu m$, $80 \mu m$, and $320 \mu m$



160 mN for PC. For LDPE a loading rate of 2 mN/s and maximum loads of 8 mN, 16 mN, and 32 mN were used. The loads held at unload were 5 mN for PMMA and PC, and 2 mN for LDPE.

3.5.3 Step 3: extract viscoelastic response

The material's viscoelastic response in this study is extracted from a ramp and hold test using the method presented by Oyen (2005). The loading conditions can be written as

$$P(t) = kt 0 \le t \le t_h$$

$$P_{\text{max}} = kt_h t_h < t \le t_u (10)$$

where t_h is the time taken to reach the maximum load and k is the loading rate. This means that the viscoelastic equation for creep (Eq. (1)) must be solved for the ramp and the hold. These solutions can be expressed as

$$h^{\frac{3}{2}}(t) = \frac{3(1-\nu)}{8\sqrt{R_{\text{eff}}}} \int_{0}^{\min(t,t_h)} J(t-\tau)kd\tau$$
 (11)

Equation (6) can then be substituted into Eq. (11) and fit to the measurements to extract the creep compliance function. This method explicitly accounts for the ramp before the hold, rather than assuming it is fast enough to be considered a step load. The relaxation modulus can then be extracted by using Eq. (8) using deconvolution techniques (Cirnu 2010; Kreyszig 2010).

In this work, the viscoelastic indentation responses were measured using ramp and hold tests on all three materials using three different indenter tip radii. For each material, the load was increased to three different loads at a constant loading rate, held for 300 seconds, and then unloaded at a constant unloading rate. The viscoelastic properties were extracted from the hold portion.

3.5.4 Step 4: perform zero point correction

As mentioned earlier, the identification of the effective zero-point is central to extracting a meaningful and reliable indentation stress-strain curve (Kalidindi and Pathak 2008; Donohue et al. 2012; Fischer-Cripps 2000; Moseson et al. 2008; Moseson et al. 2009). The central challenge comes from the fact that the machine-identified zero-point (using built-in software provided by the manufacturer) is usually incorrect. This is particularly important if our goal is to obtain reliable indentation stress-strain curves. This difference is illustrated in Fig. 3. Combining Eqs. (1) and (3), and introducing a correction to the zero-point displacement (h^*) results in

$$h(t) = \tilde{h}(t) - h^* = \frac{3(1-\nu)}{8a(t)} \int_0^t J(t-\tau) \frac{dP(\tau)}{d\tau} d\tau$$
 (12)

where $\tilde{h}(t)$ is the indentation depth measured by the machine, and h(t) is the corrected indentation depth. The zero-point correction can be easily estimated from Eq. (12) through linear regression, if we have information on the creep compliance (from step 3) and the contact radius.

In the elastic indentation, the contact radius is estimated using CSM and Eq. (4). In these protocols, stiffness is estimated through the analyses of the superimposed oscillations by the



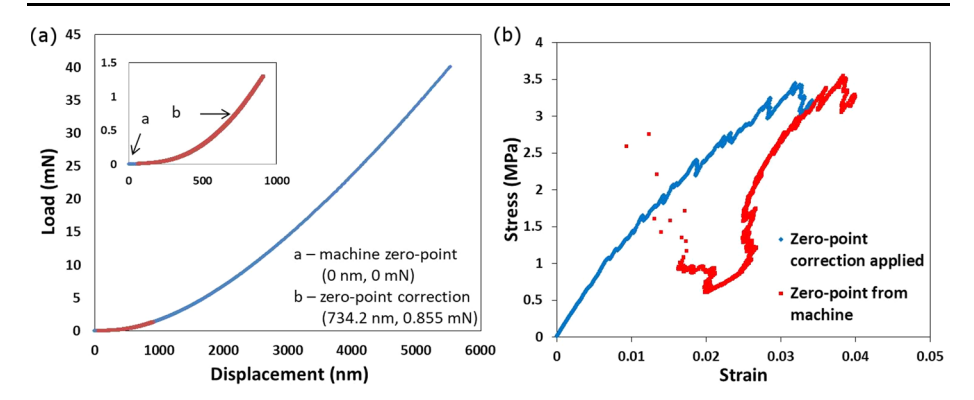


Fig. 3 a) Load-displacement curve from indentation test on LDPE. Points labeled a and b on the curve denote the machine identified zero-point and the effective zero-point identified using the protocols presented in this work, respectively. **b**) Indentation stress-strain curves extracted using the two different zero-points identified in (a)

CSM module. In the application of CSM to the viscoelastic response, one needs to verify if the measurements are sensitive to the applied frequency of the superimposed oscillations. For the present study, the oscillations applied in CSM were simulated using the FE indentation model (with the viscoelastic properties measured in this study for LDPE as these samples produced the largest viscoelastic responses as shown later) at a range of frequencies. Selected results from these simulations are presented in Fig. 4. The phase angle between the applied displacement oscillations and the resulting load oscillations were extracted from these simulations. At high frequencies, the phase angle between the oscillations approached zero, indicating that one can idealize these as elastic response (Gutierrez-Lemini 2014; Mase 1970). Therefore, we expect the relationship between the effective elastic modulus, contact area, and stiffness shown in Eq. (4) to hold at high frequencies. In the work presented here, the CSM oscillations were imposed at a frequency of 45 Hz and amplitude of 2 nm. These specific values were identified in prior work (Vachhani et al. 2013) to provide the most reliable results for the CSM.

Another important relationship that needs to be evaluated critically using the FE simulations is the relationship between contact radius, displacement, and effective radius given by Eq. (3). This is because the contact radius can be extracted directly in the FE simulation through the contact definition. The results of such an investigation are presented in Fig. 5 for both the elastic and the viscoelastic cases; four different displacement rates were examined for the viscoelastic case. These results show that, as the indenter is pushed into the material, the contact radius does not depend on the rate of indentation and is the same as the elastic case. In other words, the contact radius depends only on the indentation depth as expressed in Eq. (3). It should be noted that Eq. (3) is a geometric relation, and in the viscoelastic correspondence principle, such relationships are generally unaffected when ones goes from the elastic solution to the viscoelastic solution. In the present study, we have confirmed this with the FE simulations.

3.5.5 Step 5: extract stress-strain curves

The indentation stress-strain curves can be recovered from the load-displacement data using suitable definitions of indentation stress and indentation strain (Kalidindi and Pathak 2008;



Fig. 4 Finite element simulations for indentations on LDPE at displacement oscillation frequencies of 1 Hz, 10 Hz, and 100 Hz. The phase angle, Φ , is between the applied displacement oscillations and the resulting load oscillations

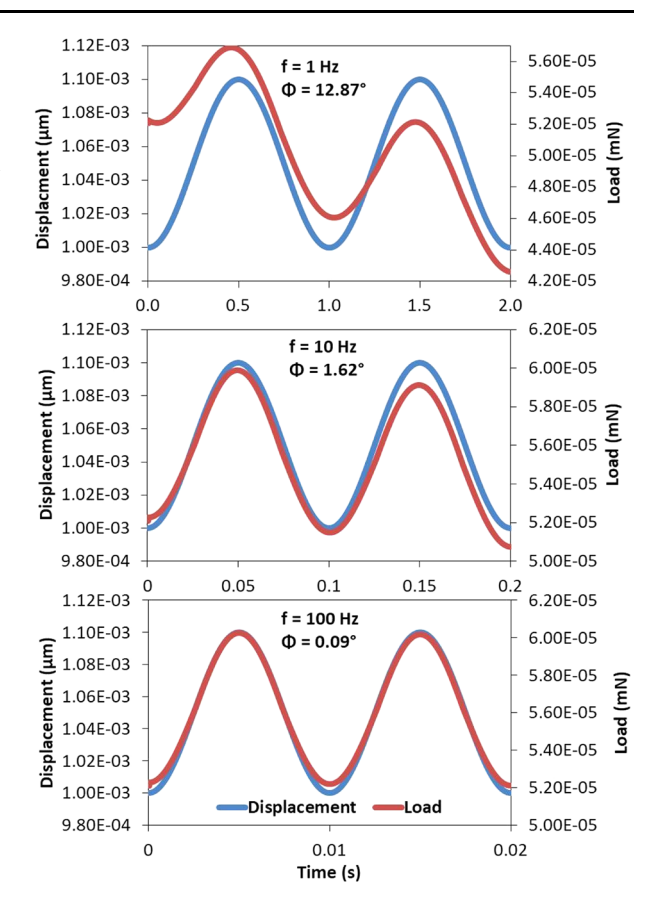
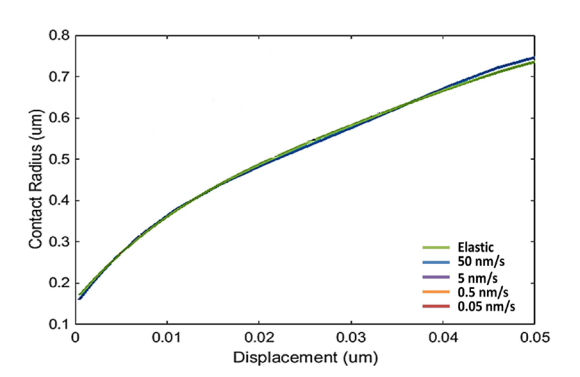


Fig. 5 Contact area versus displacement from FE simulations of indentations on LDPE at different displacement rates



Donohue et al. 2012). The indentation stress is defined classically as the load applied over the projected contact area,

$$\sigma_{ind}(t) = \frac{P(t)}{\pi a(t)^2} \tag{13}$$



Indentation strain is defined as (Kalidindi and Pathak 2008)

$$\varepsilon_{ind}(t) = \frac{4}{3\pi} \frac{h(t)}{a(t)} \approx \frac{h(t)}{2.4a(t)} \tag{14}$$

This definition of strain can be interpreted as change in length over the original length by idealizing the primary zone of indentation as a cylinder of radius, a, and length, 2.4a, which is then compressed by the indentation depth h. This definition has been validated using both numerical simulations and experimental measurements (Kalidindi and Pathak 2008; Pathak et al. 2008; Donohue et al. 2012; Pathak et al. 2009b). As mentioned earlier, the CSM oscillations can be considered elastic. Therefore, it is reasonable to estimate the contact radius throughout the test using Eq. (4), where the instantaneous relaxation modulus is used as the elastic modulus (Huang and Lu 2006). With these definitions of indentation stress and indentation strain, the load-displacement curves obtained by nanoindentation can be converted to indentation stress-strain curves.

4 Results and discussion

4.1 Uniaxial compression tests

The results from the compression tests are shown in Fig. 6. The strain rates obtained in the tests were $8 \times 10^{-4} \, \rm s^{-1}$ for PMMA and PC, and $5 \times 10^{-4} \, \rm s^{-1}$ for LDPE. It was observed that the PMMA and PC samples failed by shearing with polycarbonate shearing more than PMMA which may have caused some of the drop in stress with increasing strain. This drop in stress has been reported in literature and is usually attributed to a combined effect of strain softening and thermal softening (Arruda et al. 1995). Care was taken to ensure that the sample geometry was always a right cylinder and the axis of loading was aligned, as any misalignment would increase the shear on the material. The moduli, measured from the initial linear portion of the true stress-strain curves, were $1.9 \pm 0.031 \, \rm GPa$, $1.42 \pm 0.031 \, \rm GPa$, and $0.154 \pm 0.0014 \, \rm GPa$ for PMMA, PC, and LDPE, respectively. These results will be compared to the indentation stress-strain curves collected at similar strain rates.

4.2 Spherical nanoindentation

4.2.1 Material viscoelasticity

The results from the indentations at two different rates $(0.05 \text{ s}^{-1} \text{ and } 0.5 \text{ s}^{-1})$ using the 16 µm radius indenter on PMMA, PC, and LDPE are shown in Fig. 7. It is clearly seen that LDPE shows the largest viscoelastic component among the three materials, while PC is the least viscoelastic.

4.2.2 Viscoelastic region

The results from the tests performed to identify the regime of viscoelasticity for PMMA (without initiating significant plastic deformation) using the $100~\mu m$ radius indenter tip are shown in Fig. 8. The figure shows all curves for the four different maximum loads with at least five tests for each. The standard deviation for all cases was less than 5%. It is seen that above a certain load, there is a clearly observable difference in residual displacements. In other words, the material has experienced discernable plastic deformation above those loads. These results are summarized in Table 1, and are used to estimate the viscoelastic regime of the measured load-displacement curve.



Fig. 6 True stress-strain curves for a) PMMA, b) PC, and c) LDPE measured from simple compression tests on five samples each

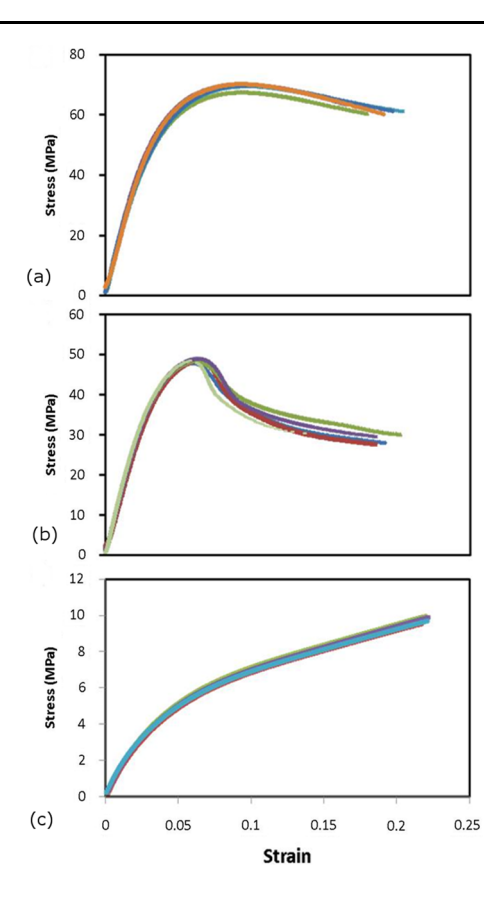


Table 1 Estimated viscoelastic load limits for the three different indenter tip radii for the samples tested in this work

Indenter size	PMMA	PC	LDPE
16 μm	40 mN	30 mN	3 mN
100 μm	160 mN	80 mN	16 mN
1500 μm	500 mN	350 mN	50 mN

4.2.3 Viscoelastic properties

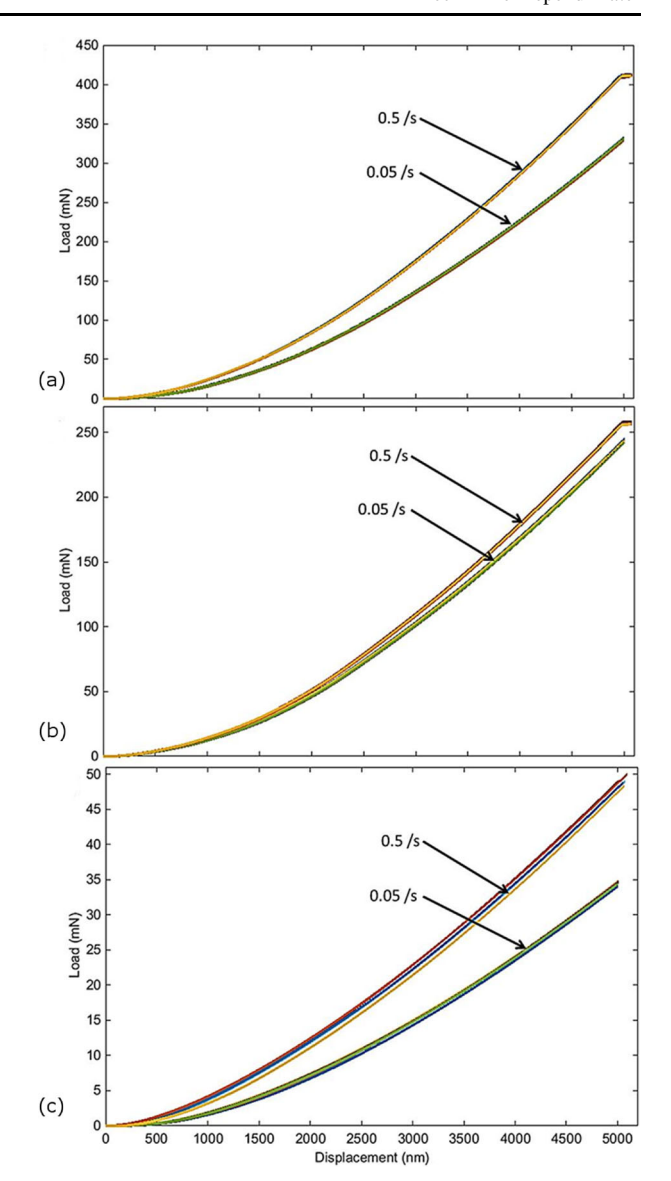
The creep compliance and corresponding relaxation modulus were extracted from the ramp and hold tests and using the methods explained in the previous section and best fits based on linear regression with five tests for each measurement. The extracted viscoelastic properties are represented in terms of a two-term Prony series, and tabulated in Table 2. The standard deviation for all cases was less than 5%. It is noted that the viscoelastic properties obtained from the tests performed with the distinctly different indenter tip radii showed reasonable agreement with each other. This agreement validates the protocols developed in this work.

4.2.4 Stress-strain curves

Once the viscoelastic properties have been extracted, the stress-strain curves can then be produced. As explained earlier, a zero-point correction for the displacement needs to be



Fig. 7 Measured indentation load-displacement curves for a) PMMA, b) PC, and c) LDPE at two different loading rates with five tests performed at each rate



established by fitting the measurements within the viscoelastic regime to Eq. (12). The zero-point correction for the load is then taken simply as the load at the corrected displacement. Since these values depend on the location of the indent, surface roughness, or other surface artifacts that may remain after polishing they should be established separately for each indentation test (even when performed on the same sample). The measured load-displacement curves are converted to stress-strain curves using the protocols described earlier. Representative results at different strain rates and different indenter tips for PMMA, PC, and LDPE are plotted in Fig. 9. The strain levels attained with the 1500 µm indenter were fairly low due to the load limit on the nanoindenter. Consequently, they covered only the very early portions of the indentation stress-strain curves shown in Fig. 9, and were seen to be in ex-



Fig. 8 Measured indentation load-displacement curves for PMMA in experiments designed to identify the viscoelastic regime. The sample is loaded to different maximum loads and unloaded to 5 mN and held while the time-dependent residual displacement is measured. The inset shows that after being loaded to 320 mN, the residual displacement is higher than the others meaning that discernable plastic deformation has occurred

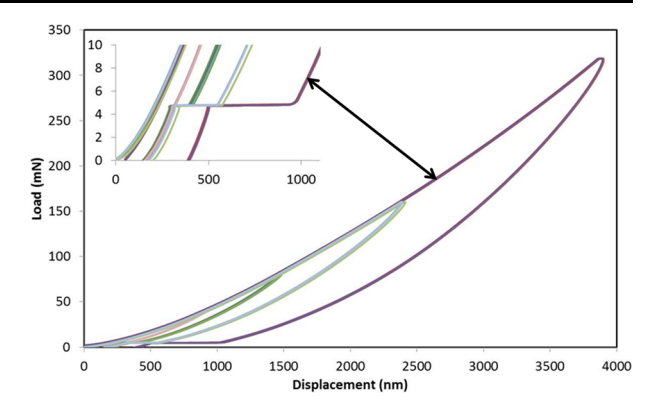


Table 2 Extracted creep compliance and relaxation modulus for the three materials studied in this work in measurements performed using three different indenter tip radii

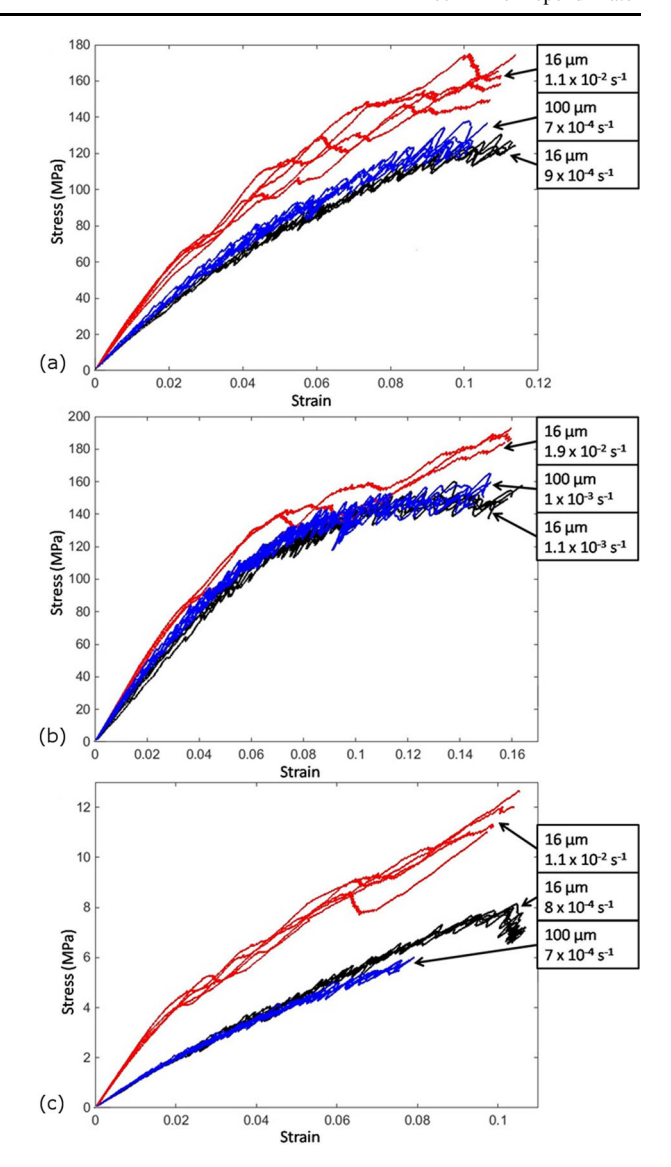
Material	Indenter size	Creep compliance (1/GPa)	Relaxation modulus (GPa)
PMMA	16 μm 100 μm 1500 μm	$0.43 - 0.032e^{-t/18} - 0.060e^{-t/216}$ $0.45 - 0.044e^{-t/15} - 0.076e^{-t/225}$ $0.41 - 0.025e^{-t/25} - 0.034e^{-t/220}$	$2.32 + 0.26e^{-t/16} + 0.37e^{-t/186}$ $2.23 + 0.37e^{-t/13} + 0.44e^{-t/187}$ $2.46 + 0.20e^{-t/23} + 0.22e^{-t/202}$
PC	16 μm 100 μm 1500 μm	$0.47 - 0.012e^{-t/15} - 0.010e^{-t/136}$ $0.49 - 0.013e^{-t/9} - 0.014e^{-t/151}$ $0.52 - 0.021e^{-t/11} - 0.016e^{-t/162}$	$2.11 + 0.059e^{-t/15} + 0.047e^{-t/133}$ $2.03 + 0.059e^{-t/9} + 0.058e^{-t/146}$ $1.92 + 0.084e^{-t/11} + 0.061e^{-t/157}$
LDPE	16 μm 100 μm 1500 μm	$6.48 - 1.22e^{-t/17} - 1.58e^{-t/154}$ $6.76 - 1.12e^{-t/14} - 1.61e^{-t/138}$ $6.54 - 1.18e^{-t/15} - 1.73e^{-t/146}$	$0.15 + 0.072e^{-t/13} + 0.046e^{-t/118}$ $0.15 + 0.057e^{-t/11} + 0.043e^{-t/106}$ $0.15 + 0.072e^{-t/11} + 0.051e^{-t/108}$

cellent agreement with the measurements obtained with the smaller indenter tips. In order to maintain the clarity of the figures, these were not included in these plots. Two particular trends are clearly seen from the results presented in Fig. 9: (i) there is remarkable agreement between the indentation stress-strain curves measured using indenter tips of vastly different radii, and (ii) the indentation stress-strain curves exhibit the expected strain rate sensitivity inferred from Step 1 (see Fig. 7). When the ratios of the stresses of the viscoelastic region for the 16 µm at the two strain rates are compared we get an average of 1.14 for PMMA, 2.22 for PC, and 1.31 for LDPE. The ratios obtained using FE simulations were 1.25 for PMMA, 2.26 for PC, and 1.31 for LDPE. These results validate the protocols presented in this work, including the normalizations implied in the indentation stress and strain measures employed, and point to their tremendous potential in studies of multiscale material response.

Comparing the indentation stress-strain curves in Fig. 9 with the simple compression stress-strain curves in Fig. 6, we observe that the indentation stress-strain curves are higher for all three materials studied in this work. This, of course, is expected because of at least two factors: (i) the higher levels of hydrostatic pressure in indentation cause the effective indentation moduli to be higher than in simple compression, and (ii) most polymers exhibit a pressure-dependent yield that further increases the indentation yield strengths as compared to the simple compression yield strengths (Spitzig and Richmond 1979). It is therefore instructive to compare these values quantitatively to derive new insights into the mechanical response of the polymers studied. In the case of rate-independent isotropic elastic-plastic



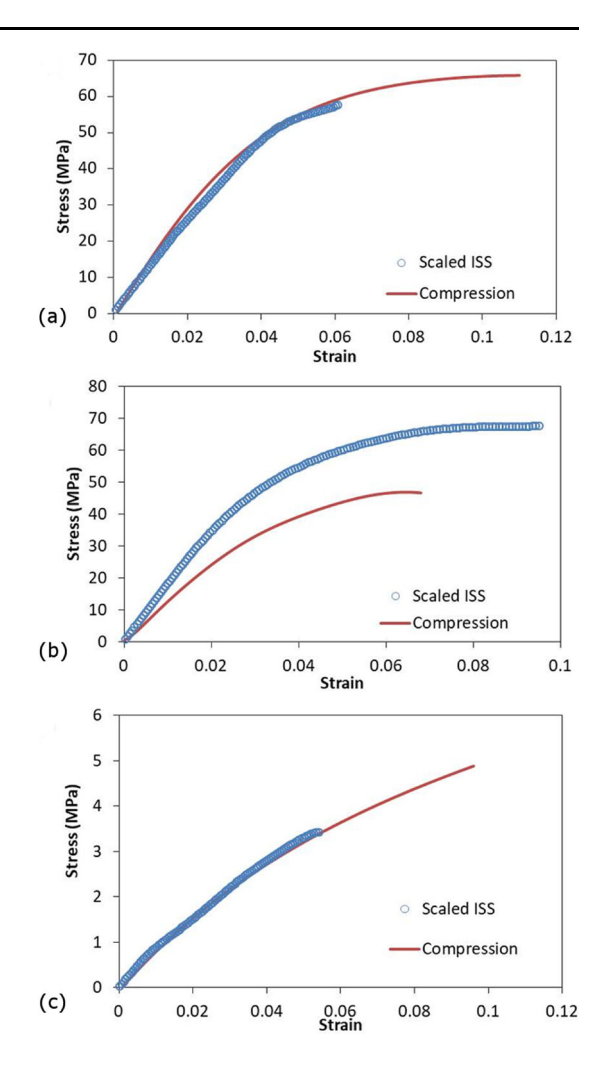
Fig. 9 Comparison of the measured indentation stress-strain curves at different loading rates with different indenter tip radii for a) PMMA, b) PC, and c) LDPE



deformation in metals, it was seen that the conversion of indentation stress-strain (ISS) curves to the simple compression stress-strain curves could be accomplished using three simple factors (Patel and Kalidindi 2016). In this prior work, the ratio between the indentation stress and uniaxial stress was found to be 2.2, the ratio between the indentation elastic strain and the uniaxial elastic strain was found to be 2, and the ratio between the indentation plastic strain and uniaxial plastic strain was found to be 1.3. We used the same factors to scale our indentation stress-strain curves and compared them to the compression stress-strain curves for PMMA, PC, and LDPE in Fig. 10. The curves obtained using the 16 μ m indenter with strain rates of $9 \times 10^{-4} \, \text{s}^{-1}$, $1.1 \times 10^{-3} \, \text{s}^{-1}$, and $8 \times 10^{-4} \, \text{s}^{-1}$ for PMMA, PC, and LDPE, respectively, were used for the scaling. It can be seen that there is good agreement between the curves for PMMA and LDPE, but not for PC. These results are



Fig. 10 A comparison of the scaled indentation stress-strain curve with the compression stress-strain curve for a) PMMA, b) PC, and c) LDPE



somewhat surprising because one would have expected the scaling factors to change for the different materials depending on the degree of pressure-dependence exhibited by them. Indeed, PC is likely to exhibit a high level of pressure-dependent yield (Caddell et al. 1974; Bahr et al. 1998), even with low levels of viscoelasticity. Clearly, more measurements on additional material systems are needed to clarify the scaling factors.

5 Conclusions

A set of protocols were presented to reliably extract viscoelastic properties and indentation stress-strain curves from spherical nanoindentation, and validated using three different indenter tip sizes on three different commercially available polymers – PMMA, PC, and LDPE. The viscoelastic indentation properties obtained with the different indenter tips were found to be remarkably consistent across all three indenter sizes for each polymer material. The indentation stress-strain curves were also compared at two different strain rates



and the measured strain rate dependence agreed well with the FE results. It was also noted that LDPE was the most viscoelastic and PC was the least viscoelastic. All of these results validate the protocols presented in this work for viscoelastic materials.

The indentation stress-strain curves at the lower strain rate were also compared to the compression stress-strain curves. It was also shown that the uniaxial compression stress-strain curve can be recovered from the indentation stress-strain curve for PMMA and LDPE by using the three scaling factors developed in prior work for elastic-plastic pressure-independent material behavior. For PC, a different set of scaling factors are needed. Although it is suspected that this is a consequence of pressure-dependent inelastic deformation in PC, it is clear that further detailed studies involving a number of other polymers are needed to fully explain this observation.

The overall goal of this paper was to provide a comprehensive workflow for studying constitutive response in viscoelastic-viscoplastic materials. We therefore defined a workflow comprising a total of five steps that end in meaningful indentation stress-strain curves that can be compared to uniaxial stress-strain curves. To the best of our knowledge, no one has actually put together the protocol described in this paper with comparable end results. We believe that comprehensive workflows are useful to move towards standardization of characterization tasks, and eventually to potential automation. Therefore, there is tremendous value to the research community is formalizing all the steps involved in the workflow.

Acknowledgements The authors gratefully acknowledge support from the National Science Foundation (Grant# NSF 1761406).

Publisher's Note Springer Nature remains neutral with regard to jurisdictional claims in published maps and institutional affiliations.

References

- Arruda, E.M., Boyce, M.C., Jayachandran, R.: Effects of strain rate, temperature and thermomechanical coupling on the finite strain deformation of glassy polymers. Mech. Mater. 19(2), 193–212 (1995)
- ASTM D695-10: Standard Test Method for Compressive Properties of Rigid Plastics. ASTM International (2010)
- Bahr, D.F., Watkins, C.M., Kramer, D.E., Gerberich, W.W.: Yield point phenomena during indentation. In: Fundamentals of Nanoindentation and Nanotribology. Symposium, 13-17, vol. 522, pp. 83–88. Mater. Res. Soc., Warrendale, PA, USA (1998). 1998
- Bouzakis, K.D., Michailidis, N., Hadjiyiannis, S., Skordaris, G., Erkens, G.: Continuous FEM simulation of the nanoindentation: actual indenter tip geometries, material elastoplastic deformation laws and universal hardness. Z. Met.kd. 93(9), 862–869 (2002)
- Brinson, H., Brinson, C.: Polymer Engineering Science and Viscoelasticity: An Introduction. Springer, New York (2008)
- Briscoe, B.J., Fiori, L., Pelillo, E.: Nano-indentation of polymeric surfaces. J. Phys. D, Appl. Phys. 31(19), 2395 (1998)
- Caddell, R.M., Raghava, R.S., Atkins, A.G.: Pressure dependent yield criteria for polymers. Mater. Sci. Eng. 13(2), 113–120 (1974)
- Cheng, Y.T., Cheng, C.M.: Relationships between initial unloading slope, contact depth, and mechanical properties for spherical indentation in linear viscoelastic solids. Mater. Sci. Eng.: A **409**(1–2), 93–99 (2005a)
- Cheng, Y.T., Cheng, C.M.: Relationships between initial unloading slope, contact depth, and mechanical properties for conical indentation in linear viscoelastic solids. J. Mater. Res. 20(4), 1046–1053 (2005b)
- Cheng, L., Xia, X., Scriven, L.E., Gerberich, W.W.: Spherical-tip indentation of viscoelastic material. Mech. Mater. 37(1), 213–226 (2005)
- Cirnu, M.I.: Linear discrete convolution and its inverse. Part 2. Deconvolution. J. Inf. Syst. Oper. Manag. 4(2), 43–55 (2010)
- Dassault Systemes Simulia Corp.: ABAQUS. In: Providence, RI, USA, (2014)



- Donohue, B.R., Ambrus, A., Kalidindi, S.R.: Critical evaluation of the indentation data analyses methods for the extraction of isotropic uniaxial mechanical properties using finite element models. Acta Mater. **60**(9), 3943–3952 (2012)
- Fischer-Cripps, A.C.: A review of analysis methods for sub-micron indentation testing. Vacuum **58**, 569–585 (2000)
- Fischer-Cripps, A.C.: Nanoindentation. Mechanical Engineering Series. Springer, New York (2002)
- Gauthier, M.M.: Engineered Materials Handbook. ASM International, Russel, Township, OH (1995)
- Graham, G.A.C.: The contact problem in the linear theory of viscoelasticity. Int. J. Eng. Sci. 3(1), 27–46 (1965)
- Gutierrez-Lemini, D.: Engineering Viscoelasticity. Springer, New York (2014)
- Hemker, K.J., Sharpe, W.N.: Microscale characterization of mechanical properties. In: Annual Review of Materials Research, vol. 37, pp. 93–126. Annual Reviews, Palo Alto (2007)
- Huang, G., Lu, H.: Measurement of Young's relaxation modulus using nanoindentation. Mech. Time-Depend. Mater. 10(3), 229–243 (2006)
- Huang, G., Lu, H.: Measurements of two independent viscoelastic functions by nanoindentation. Exp. Mech. 47(1), 87–98 (2007)
- Huang, G., Wang, B., Lu, H.: Measurements of viscoelastic functions of polymers in the frequency-domain using nanoindentation. Mech. Time-Depend. Mater. 8(4), 345–364 (2004)
- Hunter, S.C.: The Hertz problem for a rigid spherical indenter and a viscoelastic half-space. J. Mech. Phys. Solids 8(4), 219–234 (1960)
- Jäger, A., Lackner, R.: Identification of viscoelastic model parameters by means of cyclic nanoindentation testing. Int. J. Mater. Res. 99(8), 829–835 (2008)
- Jakes, J.E., Lakes, R.S., Stone, D.S.: Broadband nanoindentation of glassy polymers: Part I. Viscoelasticity. J. Mater. Res. 27(2), 463–474 (2012)
- Jaya, N.B., Alam, M.Z.: Small-scale mechanical testing of materials Curr. Sci. 105(8), 1073–1099 (2013)
- Kalidindi, S.R., Pathak, S.: Determination of the effective zero-point and the extraction of spherical nanoindentation stress-strain curves. Acta Mater. 56(14), 3523–3532 (2008)
- Kalidindi, S.R., Mohan, S., Rossi, A.: Mechanical characterization of mesoscale interfaces using indentation techniques. JOM 69(1), 22–29 (2017)
- Khosravani, A., Caliendo, C.M., Kalidindi, S.R.: New insights into the microstructural changes during the processing of dual-phase steels from multiresolution spherical indentation stress-strain protocols. Metals **10**(1), 18 (2020)
- Knauss, W.G., Emri, I., Lu, H.: Mechanics of polymers: viscoelasticity. In: Sharpe, W.N. (ed.) Springer Handbook of Experimental Solid Mechanics, pp. 49–95. Springer, Boston (2008)
- Kreyszig, E.: Advanced Engineering Mathematics. Wiley, Hoboken (2010)
- Lakes, R.: Viscoelastic Materials. Cambridge University Press, Cambridge (2009)
- Lakes, R.S., Wineman, A.: On Poisson's ratio in linearly viscoelastic solids. J. Elast. 85(1), 45–63 (2006)
- Lee, E.H.: Stress analysis in viscoelastic materials. J. Appl. Phys. 27(7), 665-672 (1956)
- Lee, E.H., Radok, J.R.M.: The contact problem for viscoelastic bodies. J. Appl. Mech. 27(3), 438–444 (1960)
- Li, X., Bhushan, B.: A review of nanoindentation continuous stiffness measurement technique and its applications. Mater. Charact. 48(1), 11–36 (2002)
- Martynova, E.: Determination of the properties of viscoelastic materials using spherical nanoindentation. Mech. Time-Depend. Mater. **20**(1), 85–93 (2016)
- Mase, G.: Schaum's Outline of Continuum Mechanics. McGraw-Hill Education, New York (1970)
- Moseson, A.J., Basu, S., Barsoum, M.W.: Determination of the effective zero point of contact for spherical nanoindentation. J. Mater. Res. 23(1), 204–209 (2008)
- Moseson, A.J., Basu, S., Barsoum, M.W.: (2009). U.S. Patent Application No. 12/184,711
- Odegard, G., Gates, T., Herring, H.: Characterization of viscoelastic properties of polymeric materials through nanoindentation. Exp. Mech. **45**(2), 130–136 (2005)
- Oyen, M.L.: Spherical indentation creep following ramp loading. J. Mater. Res. 20(8), 2094–2100 (2005)
- Patel, D.K., Kalidindi, S.R.: Correlation of spherical nanoindentation stress-strain curves to simple compression stress-strain curves for elastic-plastic isotropic materials using finite element models. Acta Mater. **112**, 295–302 (2016)
- Patel, D.K., Kalidindi, S.R.: Estimating the slip resistance from spherical nanoindentation and orientation measurements in polycrystalline samples of cubic metals. Int. J. Plast. 92, 19–30 (2017)
- Pathak, S., Kalidindi, S.R.: Spherical nanoindentation stress-strain curves. Mater. Sci. Eng. R 91, 1-36 (2015)
- Pathak, S., Kalidindi, S.R., Klemenz, C., Orlovskaya, N.: Analyzing indentation stress–strain response of LaGaO3 single crystals using spherical indenters. J. Eur. Ceram. Soc. 28(11), 2213–2220 (2008)
- Pathak, S., Stojakovic, D., Doherty, R., Kalidindi, S.R.: Importance of surface preparation on the nanoindentation stress-strain curves measured in metals. J. Mater. Res. 24(3), 1142–1155 (2009a)



- Pathak, S., Stojakovic, D., Kalidindi, S.R.: Measurement of the local mechanical properties in polycrystalline samples using spherical nanoindentation and orientation imaging microscopy. Acta Mater. 57(10), 3020–3028 (2009b)
- Pharr, G.M., Strader, J.H., Oliver, W.C.: Critical issues in making small-depth mechanical property measurements by nanoindentation with continuous stiffness measurement. J. Mater. Res. 24(3), 653–666 (2009)
- Spitzig, W., Richmond, O.: Effect of hydrostatic pressure on the deformation behavior of polyethylene and polycarbonate in tension and in compression. Polym. Eng. Sci. 19(16), 1129–1139 (1979)
- Srikar, V.T., Spearing, S.M.: A critical review of microscale mechanical testing methods used in the design of microelectromechanical systems. Exp. Mech. 43(3), 238–247 (2003)
- Ting, T.C.T.: The contact stresses between a rigid indenter and a viscoelastic half-space. J. Appl. Mech. 33(4), 845–854 (1966)
- Vachhani, S.J., Doherty, R.D., Kalidindi, S.R.: Effect of the continuous stiffness measurement on the mechanical properties extracted using spherical nanoindentation. Acta Mater. 61(10), 3744–3751 (2013)
- Vachhani, S.J., Doherty, R.D., Kalidindi, S.R.: Studies of grain boundary regions in deformed polycrystalline aluminum using spherical nanoindentation. Int. J. Plast. 81, 87–101 (2016)
- Weaver, J.S., Kalidindi, S.R.: Mechanical characterization of Ti-6Al-4V titanium alloy at multiple length scales using spherical indentation stress-strain measurements. Mater. Des. 111, 463–472 (2016)
- Zhou, Z., Lu, H.: On the measurements of viscoelastic functions of a sphere by nanoindentation. Mech. Time-Depend. Mater. **14**(1), 1–24 (2010)

